

# Solid–fluid equilibrium for a molecular model with short ranged directional forces

C. Vega

*Departamento de Química Física, Facultad de Ciencias Químicas, Universidad Complutense, 28040 Madrid, Spain*

P. A. Monson<sup>a)</sup>

*Department of Chemical Engineering, University of Massachusetts, Amherst, Massachusetts 01003*

(Received 19 June 1998; accepted 3 September 1998)

The phase diagram of a system of hard spheres with short-range tetrahedral association has been determined by computer simulation and theory. The fluid phase and two solid phases were considered. One of these solid phases is a low-density solid closely related in structure to ice Ic and the other is a high-density solid closely related in structure to ice VII. At high temperatures freezing occurs into the high-density solid whereas at low temperatures freezing occurs into the low-density solid. At an intermediate temperature a triple point is found where the fluid coexists with the two solids simultaneously. Although the low-density solid melts to a high-density fluid, this transition is found to be metastable with respect to the transformation into a high-density solid. This is evidence that short-range tetrahedral attractive forces are not in and of themselves sufficient to explain the anomalous melting of water. Our results indicate that vapor–liquid equilibrium for the model is preempted by solidification. Monte Carlo simulation results for the fluid phase are described successfully by Wertheim's theory whereas those of the solid phases are described qualitatively by the cell theory. © 1998 American Institute of Physics. [S0021-9606(98)52346-X]

## I. INTRODUCTION

Although the solid–fluid equilibrium of model potentials for simple molecules such as the hard sphere and Lennard-Jones potentials was studied over thirty years ago<sup>1,2</sup> it is only relatively recently that the solid–fluid equilibrium of non-spherical molecular models has received comprehensive attention. Frenkel and Mulder<sup>3</sup> determined the phase diagram of hard ellipsoids as a part of a study focused primarily on the nematic to isotropic phase transition. In this decade the solid–fluid equilibrium of hard spherocylinders have been determined by Jackson *et al.*<sup>4</sup> and by Bolhuis and Frenkel.<sup>5</sup> For hard dumbbells the fluid–solid equilibrium has been determined by Singer<sup>6</sup> and by ourselves.<sup>7–9</sup> Other studies of solid–fluid equilibrium for nonspherical molecules have included quadrupolar hard dumbbells,<sup>10</sup> a nonlinear triatomic hard-sphere model of propane,<sup>11</sup> ionic systems,<sup>12</sup> and freely jointed chains of tangent hard spheres.<sup>13</sup> Some ideas on the role played by shape, polarity, chain flexibility, and ionic forces in the fluid–solid equilibrium are emerging from these studies.

The studies above do not address the issue of how solid–fluid equilibrium is influenced by short-range directional forces present in hydrogen bonded systems such as water. The study of the liquid–solid transition for simple models of water have received attention recently. The formation of crystals from the fluid phase has been considered by Svishchev and Kusalik.<sup>14</sup> Also Baez and Clancy have determined by simulation the fluid–solid transition for a simple model of

water.<sup>15,16</sup> Speedy<sup>17</sup> has studied the dense phases of a simple tetravalent network forming model system using molecular dynamics. This model exhibits several interesting features including a transition from an icelike phase a more dense amorphous structure. This behavior resembles the melting of ice Ih under pressure. A key feature of Speedy's model is the presence of repulsions between pairs of nonbonded molecules in the network. These repulsions are sufficiently long ranged to act between next nearest neighbors. Speedy argues that this is the key ingredient in the model which allows it to mimic the high-density behavior of water. A less attractive feature of the model is that the connectivity of the network is permanent. This feature is presumably acceptable for the properties of the solid but seems less appropriate for the liquid where fluctuations in the network connectivity are more important. Indeed there is evidence that the crystal to amorphous phase transition in Speedy's model terminates at a critical point.<sup>17</sup>

In this paper we describe studies of solid–fluid equilibrium in a molecular model introduced by Kolafa and Nezbeda.<sup>18</sup> The model exhibits short-ranged repulsion and short-ranged directional forces which are saturated when the molecules are tetrahedrally coordinated. Thus the model is capable of describing the effects of association. Moreover network formation is reversible so that changes in connectivity associated with first-order phase transitions can be modeled. The model has been used successfully to describe some structural features of liquid water and the phase diagram of binary mixtures including water as one of the components.<sup>19–22</sup>

The primary tool we use to study the model is Monte

<sup>a)</sup>Electronic mail: monson@ecs.umass.edu

Carlo simulation. However, we also examine the applicability of two theoretical approaches. For the fluid phase we investigate the accuracy of Wertheim's thermodynamic perturbation theory.<sup>19,20,23-25</sup> For the solid phase we shall use cell theory.<sup>26</sup> It has been found recently that the cell theory provides a fair description of the solid phase of a variety of systems including hard spheres, hard-sphere mixtures,<sup>27,28</sup> Lennard-Jones, hard dumbbells,<sup>29</sup> quadrupolar hard dumbbells,<sup>30</sup> and ionic systems.<sup>12</sup>

In our work we have considered three phases: A fluid phase and two solid phases. One solid phase has tetrahedral coordination of the molecules and resembles the ice Ic phase. The other solid phase has a higher density and resembles the ice VII structure. These two choices do not exhaust the possibilities for solid structures in this system but are representative of the low-density and high-density solid phases formed by water. At high temperature the model exhibits equilibrium between the fluid and the high-density solid phase. At lower temperatures equilibrium between the fluid and the low-density solid is observed and between the low- and high-density solids. Equilibrium between the low-density solid and a fluid of higher density (corresponding to expansion on freezing) has been calculated but the equilibrium phases are metastable with respect to coexistence of the fluid and high-density solid phases. This would indicate that short-ranged directional forces are not in themselves sufficient to explain the anomalies in the solid–fluid equilibrium of water. The vapor–liquid coexistence region for the model has been calculated using the Wertheim thermodynamic perturbation theory. The results indicate that vapor–liquid coexistence is preempted by solid–fluid coexistence in a manner similar to that previously observed for systems of hard spheres with spherically symmetric short ranged attractions.<sup>39</sup>

The outline of this paper is as follows. In Sec. II we describe the molecular model, the Monte Carlo simulations, the solid phases considered and the methodology for calculating solid phase free energies. Our applications of Wertheim's thermodynamic perturbation theory and the cell theory are described in Sec. III. Our results are presented in Sec. IV and the our conclusions in Sec. V.

## II. MOLECULAR MODELS AND SIMULATION DETAILS

### A. Molecular model

The model used in this work was proposed by Kolafa and Nezbeda<sup>18</sup> as a reference system for perturbation theory studies of water and other hydrogen bonded systems. This model consists of a hard sphere of diameter  $\sigma$ , with four additional interaction sites. These four interaction sites are disposed in a tetrahedral geometry. Two of them (denoted for convenience as hydrogen sites) are located on the surface of the hard sphere (i.e., the distance to the center of the sphere is  $0.5\sigma$ ). The other two sites (denoted for convenience as electron sites) are located at a distance  $\nu$  from the center of the sphere. In this work we use  $\nu=0.45\sigma$ . There is no interaction between either two hydrogen sites or two electron sites. However, the interaction between an electron site of molecule 1 and an hydrogen site of molecule 2 is given by a square well, i.e.

$$u_{SW}(r) = -\epsilon \quad r < \lambda\sigma \\ = 0 \quad r > \lambda\sigma. \quad (1)$$

In this work two values of  $\lambda$  will be used. In particular we shall use  $\lambda^* = \lambda/\sigma = 0.15$ , the value chosen by Nezbeda *et al.* in their studies, and also  $\lambda^* = 0.10$ . One advantage of using values of  $\lambda^*$  less than 0.15 is that each interaction site can form bonds with only one other interaction site (one site bonding two other sites is not possible) and there is only one bond between a pair of molecules. Following Kolafa and Nezbeda we refer to this model as the primitive model of water (PMW). Kolafa and Nezbeda<sup>18</sup> determined the second virial coefficient of the PMW model analytically, and the Boyle temperature (where the second virial coefficient vanishes) can be easily computed. For the model with  $\lambda^* = 0.15$ ,  $T_B^* = 0.134$  whereas for the model with  $\lambda^* = 0.10$ ,  $T_B^* = 0.101$  where the reduced temperature  $T^*$  has been defined as  $T^* = T/(\epsilon/k)$  where  $k$  is the Boltzmann constant.

### B. Solid structures

For the solids two different cubic structures were considered: An ice Ic like structure and an ice VII like structure. For convenience we will refer to these as the low-density solid (LDS) and high-density solid (HDS), respectively. These two structures are illustrated in Fig. 1. In the low-density solid there are 8 molecules per unit cell (4 inside the unit cell, one on each vertex, each shared with 7 neighboring unit cells, and one on each face, each shared with one neighboring unit cell) as in a diamond lattice. The orientation of the molecule within the unit cell is such that each molecule can form square well bonds with each of its four nearest neighbors. The close packed density (maximum density without hard sphere overlaps) for this structure is given by  $\rho_{cp}^* = \rho_{cp}\sigma^3 = 3^{3/2}/8 = 0.6495$  where  $\rho$  is the number density. The LDS structure corresponds to that of ice Ic.<sup>31,32</sup> We could also consider a hexagonal structure similar to the hexagonal structure of water, usually denoted as ice Ih. However, since both structures exhibit saturation with respect to network bond formation and have the same close packed density we expect little difference between their thermodynamic properties.<sup>15,33</sup> Previous studies of hard spheres<sup>34</sup> and hard dumbbells<sup>7</sup> have shown that for such systems, solid structures with the same close packed density have quite similar thermodynamic properties.

In the HDS structure there are two molecules per unit cell (one in the center of the cubic unit cell and one at each vertex, each shared with 7 neighboring unit cells). Again the orientation of the molecules is such that each molecule can form square well bonds with four of the eight nearest neighbors. The reduced close packed density of the structure is of  $\rho_{cp}^* = 3^{3/2}/4 = 1.2989$ . This structure is similar to that ice VII.<sup>31,35</sup>

As we mentioned in the Introduction there are several other solid structures which could have been considered in this work including those resembling ice III, ice V, and ice VI. On the other hand, the two structures we have chosen are representative of low-density and high density-solids with hydrogen bonding formation. On this basis we believe that

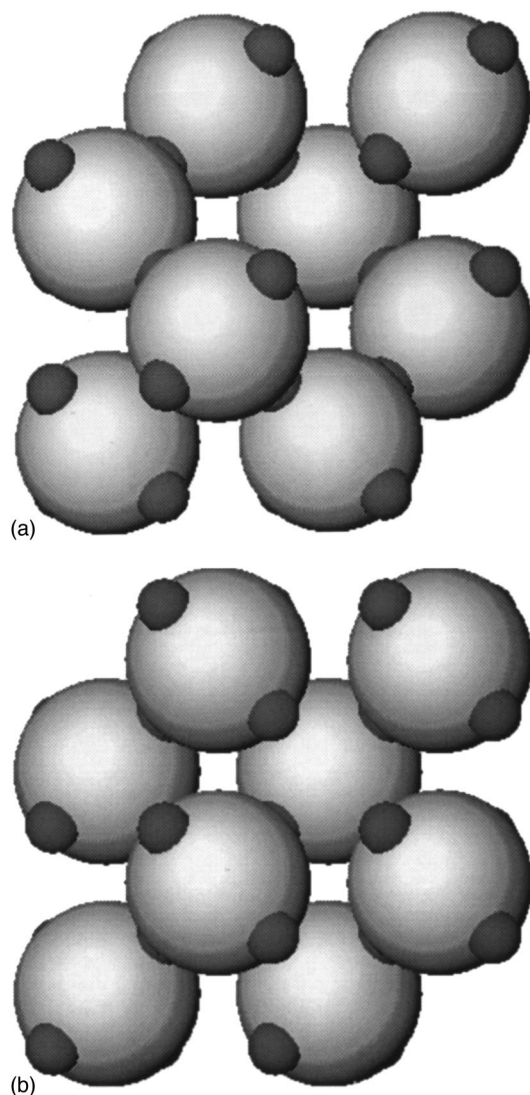


FIG. 1. Solid structures used in this work for the PMW model: (a) LDS; (b) HDS. For the LDS the eight molecules in a single unit cell are shown. For the HDS eight molecules from four unit cells are shown.

significant conclusions about the appearance of low-density solids in the phase diagrams of associating systems can be obtained from this work.

For a given value of  $\lambda^*$  there is a minimum density at which the two solid structures lose all bonds (in the perfect lattice). This density is given by

$$\rho_{\text{limit}}^* = \rho_{cp}^* / (1 + \lambda^* - 0.05)^3. \quad (2)$$

By using Eq. (2) with  $\lambda^* = 0.15$  we obtain for the low-density solid  $\rho_{\text{limit}}^* = 0.4880$  and for the HDS  $\rho_{\text{limit}}^* = 0.976$ .

### C. Monte Carlo simulations

We have performed NpT Monte Carlo (MC) simulations of the PMW in the fluid and solid phases. Since we are considering crystals of cubic symmetry we have used isotropic volume scaling. We used 216 molecules for the LDS and 128 molecules for the HDS. For the fluid phase we used both 128 and 216 molecules. We typically performed 40 000 cycles for equilibration and 40 000 cycles for obtaining av-

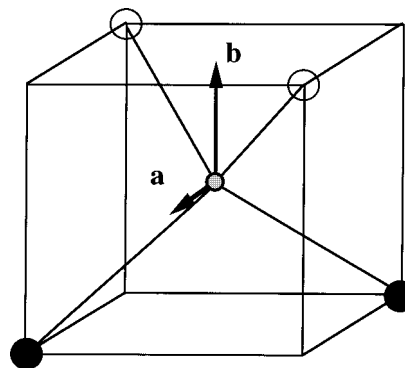


FIG. 2. Reference vectors  $\mathbf{a}_0$  and  $\mathbf{b}_0$  used in the free energy calculations.

erages. A cycle involves an attempt at moving each of the molecules of the system (translation and rotation) and an attempt to change the volume of the system. The acceptance ratio was kept in the range of 40 percent for the particle moves and of 30 percent for changes in volume. We checked the program in three different ways. First for high temperatures we reproduced the known hard-sphere results. Second we checked that the pressure obtained from the virial theorem (see Ref. 18 for the implementation of the virial theorem to the PMW model) was consistent with the input pressure of our isobaric Monte Carlo simulations. Finally, we compared our results for the pressure and internal energy of the fluid with those published previously by Kolafa and Nezbeda<sup>18</sup> and the results agree within the estimated uncertainties.

### D. Solid phase free energy calculations

To calculate solid phase free energies we implemented the Frenkel–Ladd<sup>34</sup> methodology. Further details of this methodology as applied to nonspherical molecules can be found in Ref. 3 and in our previous work.<sup>7,8,10</sup> The Einstein crystal field that was used in the simulations is given by

$$H_{\text{field}}/(kT) = \sum_{i=1}^N \left[ \lambda_{E,1} (\mathbf{R}_i - \mathbf{R}_{i,0})^2 + \lambda_{E,2} \sin^2 \psi_{a,i} + \lambda_{E,2} \left( \frac{\psi_{b,i}}{\pi} \right)^2 \right], \quad (3)$$

where  $\mathbf{R}_i$  and  $\mathbf{R}_{i,0}$  represent the location of the center of mass of molecule  $i$  for the current configuration and for the initial perfect lattice configuration, respectively. The angles  $\psi_a$  and  $\psi_b$  are defined as follows. Let  $\mathbf{a}_{i,0}$  and  $\mathbf{b}_{i,0}$  be two perpendicular unit vectors assigned to each molecule in the perfect lattice (the vectors  $\mathbf{a}$  and  $\mathbf{b}$  are shown in Fig. 2).  $\mathbf{a}_i$  and  $\mathbf{b}_i$  represent these vectors in the current configuration.  $\psi_{a,i}$  is the angle formed by the vectors  $\mathbf{a}_i$  and  $\mathbf{a}_{i,0}$  and  $\psi_{b,i}$  is the angle formed by the vectors  $\mathbf{b}_i$  and  $\mathbf{b}_{i,0}$ . The units of  $\lambda_{E,1}$  and  $\lambda_{E,2}$  are chosen so that the right hand side of Eq. (3) is dimensionless. The form of the external field used here guarantees that the energy is invariant under a symmetry operation of the molecule. For instance a rotation of 180 degrees about the  $\mathbf{b}_0$  axis exchanges the locations of the two hydrogen sites (and those of the two electron sites also). This rotation leaves the angle  $\psi_b$  unchanged but changes the angle

$\psi_a$  by  $\pi$  radians. The presence of the term  $\sin^2 \psi_a$  guarantees the invariance of the Einstein crystal energy under this symmetry operation of the molecule. In general, for rotations about a twofold axis of the molecule there should be a term in the field of the form  $\sin^2(\cdot)$  to guarantee the invariance of the energy under a 180 degree rotation. The same procedure was used for hard dumbbells<sup>7</sup> and for a nonlinear hard triatomic model of propane.<sup>11</sup>

The orientational contribution to the free energy of the reference noninteracting Einstein crystal is given by

$$\frac{A_{E,or}}{NkT} = \frac{1}{8\pi^2} \int \exp\{-\lambda_{E,2}[\sin^2 \psi_a + (\psi_b/\pi)^2]\} \times \sin \alpha d\alpha d\phi d\gamma, \quad (4)$$

where  $\alpha$ ,  $\phi$ , and  $\gamma$  are the three Euler angles defining the orientation of the molecule and the subscript  $i$  has been dropped since the integral is the same for all molecules. We follow Gray and Gubbins<sup>36</sup> in our definition of the Euler angles. By choosing the  $\mathbf{a}_0$  vector as the z axis (so that the Euler angle  $\alpha$  is identical to  $\psi_a$ ) then the integral in Eq. (4) can be further simplified to give

$$A_{E,or}/NkT = 1/(8\pi^2) \int \exp\{-\lambda_{E,2}[\sin^2 \alpha + (\psi_b/\pi)^2]\} \times \sin \alpha d\alpha d\phi d\gamma. \quad (5)$$

The angle  $\psi_b$  is in general a function of all three Euler angles, and the integral of Eq. (5) must be performed numerically. However, for large values of  $\lambda_{E,2}$  the only significant contribution to the integral arises when  $\alpha$  is close to zero. When  $\alpha$  is close to zero the angle  $\psi_b$  can be identified with the Euler angle  $\gamma$  at least up to  $\pi$ . Note that by construction the Euler angle  $\gamma$  ranges from zero to  $2\pi$  whereas we have defined  $\psi_b$  only from zero to  $\pi$ . Therefore, for large values of  $\lambda_{E,2}$ , the integrand does not depend on  $\phi$  and  $\psi_b$  can be identified with  $\gamma$  so that Eq. (5) yields

$$A_{E,or}/NkT = 1/(2\pi) \int_0^\pi \exp[-\lambda_{E,2} \sin^2 \alpha] \times \sin \alpha d\alpha \int_0^\pi \exp[-\lambda_{E,2}(\gamma/\pi)^2] d\gamma, \quad (6)$$

or simply

$$A_{E,or}/NkT = \int_0^1 \exp[-\lambda_{E,2}(1-x^2)] dx \times \int_0^1 \exp[-\lambda_{E,2}x'^2] dx', \quad (7)$$

where  $x = \cos \alpha$  and  $x' = \gamma/\pi$ . We checked that Eqs. (5) and (7) gave identical results for large values of  $\lambda_{E,2}$ . This simplification was used by Shen and Monson<sup>11</sup> in their work on a triatomic hard-sphere model of propane with large values of the force constant. The difference between the free energy of the PMW solid and that of the interacting Einstein crystal is denoted as  $\Delta A_2$  and is given by

$$\Delta A_2/(NkT) = 1/N \int_0^{\lambda_{E,max}} \left\langle \sum_{i=1}^N \left\{ [(\mathbf{R}_i - \mathbf{R}_{i,0})/\sigma]^2 + \sin^2 \psi_{a,i} + \left(\frac{\psi_{b,i}}{\pi}\right)^2 \right\} \right\rangle d\lambda, \quad (8)$$

where the angled brackets stand for canonical average over the interacting Einstein crystal.

The difference between the free energies of interacting and noninteracting Einstein crystals is obtained from

$$\Delta A_1/(NkT) = -1/N \ln \left\langle \exp \left[ - \sum_{i < j} u^{PMW}(i,j)/(kT) \right] \right\rangle, \quad (9)$$

where the brackets denote canonical ensemble average over configurations of the noninteracting Einstein crystal. The  $\Delta A_1$  term is comparable in magnitude to the internal energy of the solid. The final expression for the free energy of the PMW model is given by

$$A = A_E + \Delta A_1 + \Delta A_2 + \Delta A_3, \quad (10)$$

where  $A_E$  is the free energy of an ideal Einstein crystal,  $\Delta A_1$  is the difference between the free energy of an ideal Einstein crystal and that of the Einstein crystal with PMW interactions,  $\Delta A_2$  is the difference in free energy between the PMW solid and an Einstein crystal with PMW interactions and  $\Delta A_3$  is the difference between a system with an unconstrained center of mass and one with a fixed center of mass. Expressions for the translational contribution to  $A_E$  and for the  $\Delta A_3$  can be found elsewhere.<sup>7,34</sup>

Once the free energy has been determined for a given density and temperature the free energy at other densities or temperatures can be obtained by thermodynamic integration (using the P,V,T equation of state for changes in density and the internal energy for changes in temperature). We checked our free energy calculations by evaluating the free energies of the CsCl like solid at two different densities (i.e.,  $\rho^* = 1.171$  and  $\rho^* = 1.240$ ). Thermodynamic integration yields  $\Delta A = 1.107$ , whereas the difference in the free energy as evaluated from our free energy calculations yields  $\Delta A = 1.115$ . The difference is consistent with the statistical error in the equation of state and free energy calculations.

There is one final issue concerning the solid phase free energies for the PMW model. In the two solid structures considered so far the centers of mass and orientations of the molecules in the equilibrium solid are fixed. In the perfect solid structure each molecule has four square well bonds. However, there is the possibility of having a solid, with the same distribution of centers of mass, but with orientational disorder while keeping four hydrogen bonds per molecule. There is an additional contribution to the free energy of the solid due to this orientational disorder. This is the well-known problem of the residual entropy of ice. Pauling estimated this residual entropy to be<sup>31,37</sup>

$$A_{\text{disorder}}/NkT = -S_{\text{disorder}}/(Nk) = -\ln\left(\frac{3}{2}\right) = -0.405. \quad (11)$$

A more accurate estimate obtained by Nagle<sup>38</sup> is

$$A_{\text{disorder}}/NkT = -0.410. \quad (12)$$

These estimates are sufficiently close that the choice of either one does not affect the calculation of the phase diagram within the uncertainties of our calculations. Our strategy is to estimate the free energy of the solid with orientational order, and then to add the contribution given by Eq. (11) to estimate the free energy of the solid with orientational disorder. A similar approach was used previously for hard dumbbells<sup>7</sup> with  $L^* = 1$ , where the possibility of configurational degeneracy in the solid also exists.

### III. THEORIES FOR FLUID AND SOLID PHASE PROPERTIES

#### A. Thermodynamic perturbation theory

The implementation of Wertheim's thermodynamic perturbation theory for the PMW model has been described by Nezbeda *et al.*<sup>19,20</sup> and we shall provide here only the main results. The free energy, internal energy and compressibility factor of the PMW model are given according to Wertheim's theory by

$$\frac{A}{NkT} = \frac{A_{HS}}{NkT} + \frac{2c}{1+c} - 4 \ln(1+c), \quad (13)$$

$$\frac{U}{N\epsilon} = -\frac{2c}{1+c}, \quad (14)$$

$$Z = \frac{p}{\rho kT} = Z_{HS} - 2y \frac{1+2c}{(1+c)^2} (dc/dy), \quad (15)$$

where  $c$  is given by

$$c = 0.5 \left( \left[ 1 + 192 \left( \exp\left(\frac{1}{T^*}\right) - 1 \right) y J \right]^{0.5} - 1 \right), \quad (16)$$

and  $J$  is given by

$$J = \int_1^{\lambda-1} S(R) g_{HS}(R) R^2 dR, \quad (17)$$

where  $g_{HS}$  is the radial distribution function of hard spheres, and  $S(R)$  is the probability for a particular hydrogen bond between two molecules when the distance between the center of mass is  $R$ . This probability has been reported elsewhere [in fact it is  $\frac{1}{8}$  of Eq. (5) of Ref. 18]. We have defined the volume fraction  $y$  as

$$y = \rho \frac{\pi}{6} \sigma^3. \quad (18)$$

To compute  $J$ , an expression for  $g_{HS}$  is needed. We follow Iglesias and Nezbeda<sup>20</sup> and shall use the expression

$$g_{HS}(R) = \frac{1-0.5y}{(1-y)^3} - \frac{9y(1+y)}{2(1-y)^3} (R-1). \quad (19)$$

Replacing this expression for  $g_{HS}$  into Eq. (15) it can be shown that  $J$  can be expressed as

$$J = \frac{c_1(1-y/2) - c_2y(1+y)}{(1-y)^3}, \quad (20)$$

where the constants  $c_1$  and  $c_2$  depend on  $\lambda^*$ . (For  $\lambda^* = 0.15$ :  $c_1 = 2.375 \times 10^{-5}$  and  $c_2 = 2.820 \times 10^{-6}$ . For  $\lambda^* = 0.10$ :  $c_1 = 2.051 \times 10^{-6}$  and  $c_2 = 1.196 \times 10^{-7}$ .) The final expression for  $Z$  is then

$$Z = Z_{HS} - \frac{96(\exp(1/T^*) - 1)}{(1+c)^2} \times \frac{c_1y(1+y-0.5y^2) - 2c_2y^2(1+2y)}{(1-y)^4}. \quad (21)$$

#### B. Cell theory

Here we shall describe briefly our implementation of the cell theory for the PMW model. We refer the reader to our previous work for further details.<sup>29,30</sup> We shall start from the perfect lattice. One molecule (labeled arbitrarily as molecule 1) will be chosen as the central molecule. The interaction energy of molecule 1 with the rest of the molecules of the solid (all molecules but 1 stay in their equilibrium lattice position) is given by

$$U(1) = U^0 + \Delta U(1), \quad (22)$$

where  $U^0$  is the lattice energy of molecule 1 in its equilibrium configuration and  $\Delta U(1)$  is the change in the interaction energy of molecule 1 when it moves from the equilibrium configuration. According to the cell theory the configurational free energy of the solid is given by

$$A_{\text{cell}}^c/(NkT) = U^0/(2kT) - \ln\left(\frac{q_1}{\sigma^3}\right), \quad (23)$$

where  $q_1$  is the cell configurational partition function (free volume) and is given by

$$q_1 = 1/(8\pi^2) \int \exp(-\Delta U(1)/(kT)) d\mathbf{R}_1 d\omega_1, \quad (24)$$

where  $\mathbf{R}_1$  and  $\omega_1$  define the position and orientation of molecule 1, respectively. Equation (24) is evaluated numerically by Monte Carlo integration.<sup>29,30</sup>

### IV. RESULTS

We begin by presenting the results obtained for the fluid phase. Two temperatures were considered namely  $T^* = 0.25$  and  $T^* = 0.15$ . For the higher temperature we generally started from a low-pressure state and then compressed the system by progressively increasing the pressure. We checked that the same densities were obtained by expanding from a high-pressure fluid state. For the lower temperature we started from the states generated at  $T^* = 0.25$  and then performed five long runs slowly decreasing the temperature down to  $T^* = 0.15$ . The runs used in this cooling sequence were three times longer than those used on isotherms in order to facilitate equilibration as the temperature was decreased. In Fig. 3 the simulation results for the equation of state (EOS) and internal energy are compared with the results from the Wertheim theory for the case  $\lambda^* = 0.15$ . The agreement between theory and simulation is very good as was also shown previously by Nezbeda *et al.*<sup>19,20</sup> For temperatures lower than  $T^* = 0.15$  simulations of the fluid phase

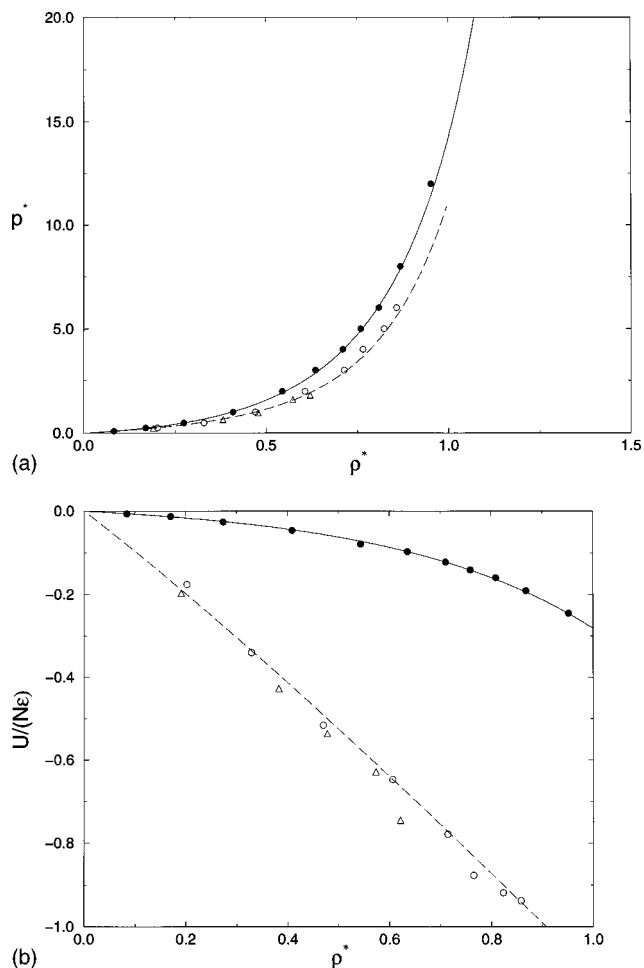


FIG. 3. Simulation and theoretical results for the equation of state and internal energy of the PMW model with  $\lambda^* = 0.15$ . MC results of this work for  $T^* = 0.25$  (filled circles), for  $T^* = 0.15$  (open circles), and from Ref. 18 for  $T^* = 0.15$  (open triangles). Results from Wertheim theory for  $T^* = 0.25$  (solid line) and  $T^* = 0.15$  (dashed line). (a) Equation of state. (b) Internal energy.

become much more difficult due to the long relaxation times of the system. Given the quality of the agreement shown in Fig. 3 we have used the Wertheim theory to calculate the fluid properties used in our phase equilibrium calculations.

According to the Wertheim theory there is a vapor–liquid equilibrium for the PMW model.<sup>20</sup> In Fig. 4 the vapor–liquid coexistence curves predicted by the theory are shown for  $\lambda^* = 0.15$  and  $\lambda^* = 0.10$ . The critical temperatures predicted for the two models are  $T^* = 0.103$  and  $T^* = 0.083$ , respectively. The critical temperature decreases with  $\lambda^*$  since the volume where attractive forces act shrinks with the range of the potential. The effect is similar to that found previously for potentials with attractive forces of spherical symmetry.<sup>39</sup> For models with short-range attractive forces it has been found that there is no vapor–liquid equilibrium. In fact Frenkel *et al.* showed that the vapor–liquid equilibrium is located inside the vapor–solid coexistence curve.<sup>39</sup> A natural question to ask is whether the the vapor–liquid equilibrium presented in Fig. 4 for the PMW is preempted by a vapor–solid transition. We shall return to this point later.

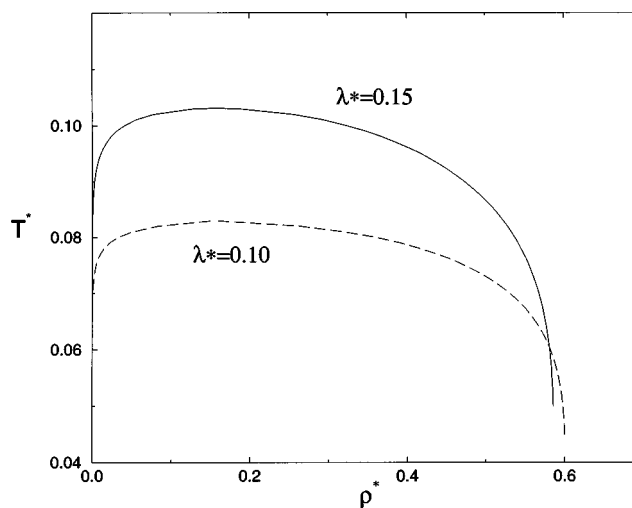


FIG. 4. Coexistence densities for vapor–liquid equilibrium in the PMW model as obtained from the Wertheim theory. Solid line:  $\lambda^* = 0.15$ , dashed line  $\lambda^* = 0.10$ .

We turn now to the simulation results for the low-density solid structure. For  $T^* = 0.25$  the low-density solid phase is not mechanically stable and it melts spontaneously. Selected results for the low-density solid are shown in Table I for the temperature  $T^* = 0.12$ . From the values of the configurational energy it is evident that there is almost complete square well bond saturation at all the densities, indicating that bond breaking is a rare event. Although not reported in

TABLE I. Results of the MC simulations of the solid phase for the PMW model with  $\lambda^* = 0.15$  and  $\lambda^* = 0.10$ . Results for the LDS and HDS are reported. Although we performed simulations at different temperatures we report here results for one temperature only. The number of molecules used in the simulations is denoted as  $N$ .

Solid	$N$	$\lambda^*$	$T^*$	$p^*$	$\rho^*$	$U/(N\epsilon)$
LDS	216	0.15	0.12	14	0.635	-1.993
LDS	216	0.15	0.12	12	0.625	-1.998
LDS	216	0.15	0.12	10	0.621	-1.999
LDS	216	0.15	0.12	8	0.616	-1.996
LDS	216	0.15	0.12	6	0.611	-1.998
LDS	216	0.15	0.12	2	0.600	-1.998
LDS	216	0.15	0.12	0.5	0.596	-1.994
HDS	128	0.15	0.12	35	1.226	-2.000
HDS	128	0.15	0.12	25	1.207	-2.000
HDS	128	0.15	0.12	20	1.198	-2.000
HDS	128	0.15	0.12	10	1.178	-2.000
HDS	128	0.15	0.12	6	1.169	-1.999
HDS	128	0.15	0.12	4	1.161	-1.999
HDS	128	0.15	0.12	0.5	1.158	-1.999
LDS	64	0.10	0.10	15	0.633	-1.999
LDS	64	0.10	0.10	10	0.629	-1.999
LDS	64	0.10	0.10	8	0.627	-1.999
LDS	64	0.10	0.10	4	0.624	-1.999
LDS	64	0.10	0.10	2	0.623	-1.999
LDS	64	0.10	0.10	0.5	0.622	-1.999
HDS	54	0.10	0.10	35	1.244	-1.999
HDS	54	0.10	0.10	25	1.239	-1.999
HDS	54	0.10	0.10	15	1.234	-1.999
HDS	54	0.10	0.10	10	1.230	-1.999
HDS	54	0.10	0.10	5	1.228	-1.999
HDS	54	0.10	0.10	0.5	1.225	-1.999

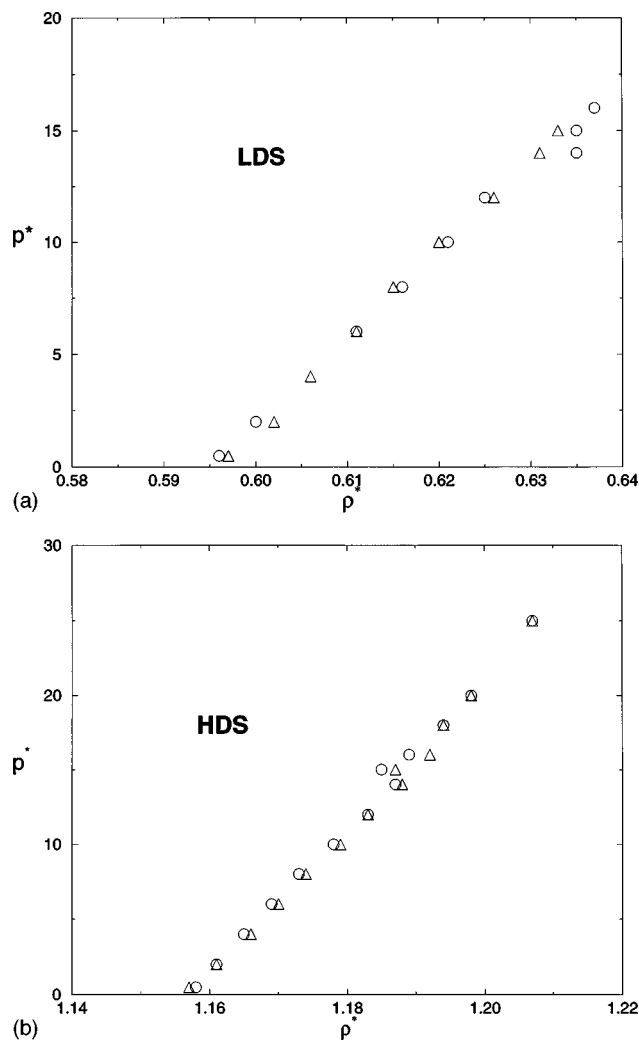


FIG. 5. Pressure vs density as obtained from MC for the PMW solid with  $\lambda^* = 0.15$ . (a) Results for the LDS with  $T^* = 0.12$  (open circles) and  $T^* = 0.075$  (open triangles). The simulation results of the LDS can be described by the equation  $p^* = -228.115 + 383.293\rho^*$ . (b) Results for the HDS at  $T^* = 0.12$  (open circles) and  $T^* = 0.075$  (open triangles). The simulation results for the HDS can be described by the equation  $p^* = -556.54 + 489.563\rho^*$ .

Table I we also performed simulations for the LDS with  $T^* = 0.075$ . Also in this case we found square well bond saturation at all the densities. In determining the temperature dependence of the free energy for our calculations of the phase diagram we use the approximation  $U/(N\epsilon) \approx -2$ . In Fig. 5(a) the reduced pressure  $p^* = p/(kT/\sigma^3)$  for the low-

density solid is plotted as a function of the density for the temperatures  $T^* = 0.12$  and  $T^* = 0.075$ . For the system size we have studied the solid is mechanically stable down to zero pressure. The variation of the pressure with density is almost linear for these temperatures. Moreover  $p/T$  is practically independent of the temperature for a given reduced density, differences lying within the simulation error. We shall use this result in our calculations of the phase diagram rather than repeat simulations of the same solid structure for many different temperatures.<sup>40</sup> It is interesting to note that the density at zero pressure for the LDS occurs at 91.63% of its close packed density. For the HDS it occurs at 89% of its close packed density. We have studied the variation with temperature of the zero pressure density for the LDS. For the temperature range studied ( $T^* = 0.005-0.12$ ) the zero-pressure density was found to be practically independent of temperature, differences being within the numerical uncertainty. Therefore, the PMW model is not able to reproduce the negative values of the thermal expansivity at atmospheric pressure found experimentally for ice for temperatures less than 50 K.<sup>31,33</sup> It is not clear whether this is due to the simplicity of the model or to the presence of quantum effects in real water for these low temperatures.

For the low-density solid we have evaluated the free energy at a reference density and temperature. Results of the free energy calculations are presented in Table II. In Fig. 6 we show the phase diagram obtained for  $T^* = 0.12$  when considering only the fluid and the low-density solid phase. The sequence of phase transitions is fluid to low-density solid to fluid, i.e., we have re-entrant behavior. It is tempting to identify this feature with the behavior of water where the ice Ih phase can coexist with a more dense liquid. In fact when compressing the low-density solid to high pressures the spontaneous melting to a high-density liquid was observed for  $T^* = 0.12$ . This is similar to the low-density solid–high-density fluid melting observed by Speedy<sup>17</sup> for a permanently connected network model. Notice, however, that the bonds in the present model are reversible and the degree of bonding in the high-density fluid is less than in the solid. However, in order to gain a wider perspective on the phase diagram we need also to consider the HDS phase.

In Table I we have also presented selected simulation results for the HDS. Results for the free energy are shown in Table II. As can be seen in Table I the configurational energy per molecule in HDS is also close to  $U/(N\epsilon) = -2$ , indicating square well bond saturation. In Fig. 5(b) the reduced

TABLE II. Free energy calculations for the LDS and HDS structures with  $\lambda^* = 0.15$  and  $\lambda^* = 0.10$ . Pauling's contribution to the free energy ( $A_{\text{disorder}}$ ) has been included in the results reported in the last column. All free energies are given in  $NkT$  units. The number of values of  $\lambda_E$  considered to perform the integration of Eq. (8) is denoted as  $N_{\lambda_E}$ . The maximum value of the field used in the free energy calculations is denoted as  $\lambda_{E,\text{max}}$ .

Solid	$\lambda^*$	$N$	$T^*$	$\rho^*$	$\lambda_{E,\text{max}}$	$N_{\lambda_E}$	$\Delta A_2$	$\Delta A_1$	$A_{\text{ref}}$
LDS	0.15	216	0.12	0.60	8000	10	-11.4328	-16.6493	-2.4636
HDS	0.15	128	0.12	1.171	8000	10	-10.636 17	-16.6627	-1.7177
HDS	0.15	128	0.12	1.240	20 000	20	-12.302 13	-16.6198	-0.6021
LDS	0.10	64	0.10	0.623	20 000	15	-10.8103	-19.9573	-2.5459
HDS	0.10	54	0.10	1.226	20 000	15	-9.7576	-19.9844	-1.5428

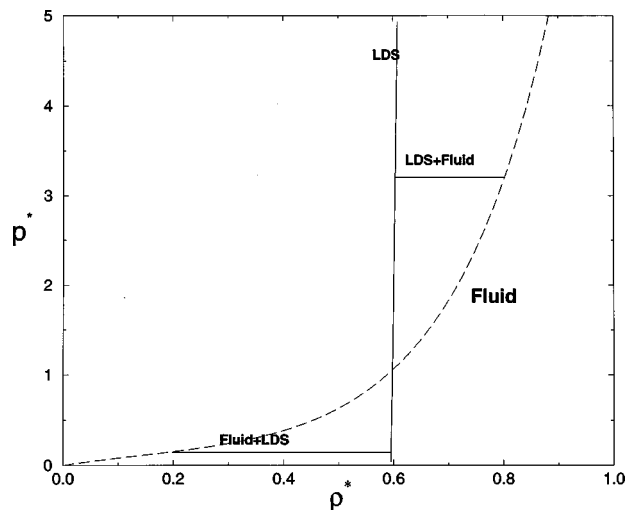


FIG. 6. Pressure vs density and phase transitions for the PMW model with  $\lambda^*=0.15$  and  $T^*=0.12$ . Only the fluid (as described by Wertheim's theory) and the LDS were considered. The tie lines correspond to the phase transitions found for this system when only these two phases are considered.

pressure is plotted as a function of the reduced density for two temperatures. Again we have found that in our simulations the solid is mechanically stable down to zero pressure. We do not observe melting even at very low pressures and with long runs. In Fig. 5(b) it can be seen that the pressure is linear and density and moreover that  $p/T$  does not depend on temperature. In Fig. 7 the phase transitions for the PMW with  $\lambda^*=0.15$  and  $T^*=0.12$  is presented. The sequence of phase transitions when increasing pressure is fluid to low-density solid to HDS. The melting of the low-density solid to a high-density fluid indicated in Fig. 6 is preempted by the low-density solid to HDS transition.

In Fig. 8(a) our estimate of the temperature-density phase diagram for the PMW with  $\lambda^*=0.15$  is presented. At

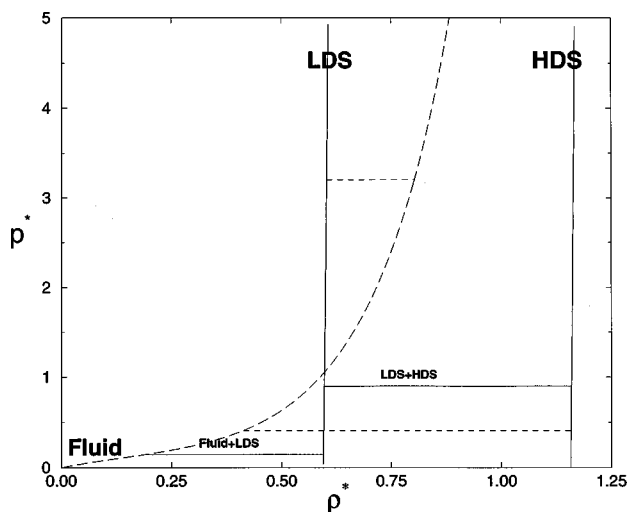


FIG. 7. Pressure vs density and phase transitions for the PMW model with  $\lambda^*=0.15$  and  $T^*=0.12$ . In this case, the fluid, the LDS and the HDS were considered. The tie lines represented by solid lines correspond to phase transitions that actually occur for this system. The tie lines represented by dashed lines correspond to phase transitions that occur between metastable phases.

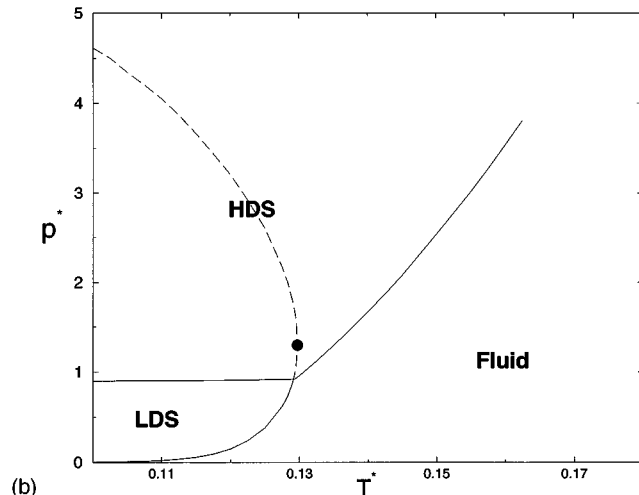
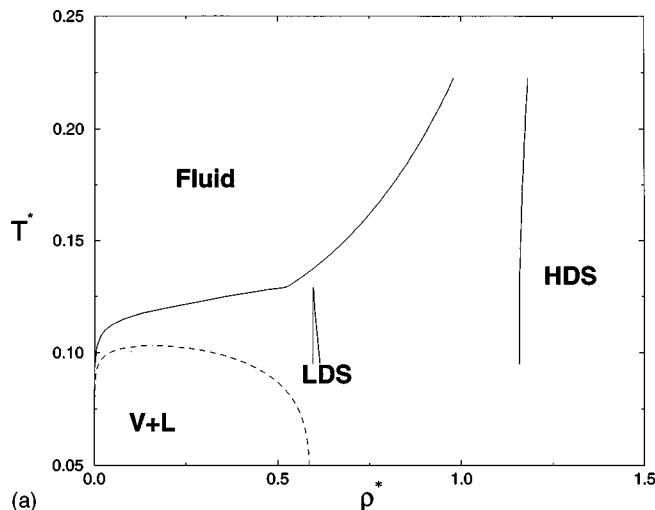


FIG. 8. Phase diagram for the PMW model with  $\lambda^*=0.15$ . (a)  $T^* - \rho^*$  diagram. The vapor-liquid equilibrium predicted by the Wertheim theory is represented by the dashed line. The densities of the LDS in the LDS-HDS solid transition have been slightly incremented with respect to the actual values for visual clarity. (b)  $p^* - T^*$  diagram showing the region of stability of each phase. The triple point where the three solid lines meet correspond to  $T^*=0.1295$  and  $p^*=0.90$ . The dashed line indicates a phase transition between the metastable fluid and the metastable LDS. The filled circle indicates the state where the transition between the metastable phases occurs without density change.

high temperatures we have a fluid to HDS transition. There is a triple point at about  $T^*=0.129$ . At lower temperatures we have first a fluid to low-density solid transition. On compressing the low-density solid we have a further transition from the low-density solid to the high-density solid. Clearly the vapor-liquid equilibrium we have calculated from the Wertheim theory occurs in a region where the fluid is not thermodynamically stable. Before condensation to liquid can occur the low-density fluid freezes into the low-density solid. The situation resembles that found for systems with spherically symmetric attractive forces of very short range (e.g., the square well potential with small values of the well width).<sup>39</sup>

In Fig. 8(b) the phase diagram is shown in a  $p^* - T^*$  diagram. At the maximum in temperature of the fluid-LDS coexistence line the density change between both phases

vanishes. This occurs at a point (filled circle) where neither of these phases is stable with respect to the HDS. From this figure it is clear that in order to have re-entrant behavior for states where the LDS phase is thermodynamically stable the coexistence line for the fluid and HDS should be pushed to higher pressures. This would require a change in the model that would render the high-density solid less stable.

We have also considered the phase diagram of the model with  $\lambda^* = 0.10$ . Our motivation is to analyze if a reduction in the range of the potential brings reentrance in the phase diagram. Since our aim is exploratory rather than quantitative in this case we have used smaller system sizes. For the low density solid 64 molecules were used in the simulations whereas for the HDS we used 54 molecules. Wertheim theory was used to describe the fluid for the PMW with  $\lambda^* = 0.10$ . In Tables I and II MC results for the PMW with  $\lambda^* = 0.10$  are shown. The phase diagram is presented in Figs. 9(a) and in 9(b). The phase diagram resembles closely that determined for  $\lambda^* = 0.15$ .

In all the calculations presented so far we have included the orientational disorder contribution as given by Eq. (11) in the free energy of the solid. It is interesting to see the effect of removing of this term on the phase diagram. In Fig. 10 the phase diagram obtained in this way is presented for the system with  $\lambda^* = 0.15$ . We see that the fluid is stable up to slightly higher densities and that freezing occurs at higher densities of the fluid (and, therefore, at higher pressures). The densities of the solid at coexistence are modified only slightly. The triple point temperature decreases when the orientational disorder contribution is not included (the triple point temperature is  $T^* = 0.123$  to be compared with  $T^* = 0.129$  with the orientational disorder contribution). Notice that the triple point is also the limit of stability of the LDS (the LDS is not stable for higher temperatures). Thus the presence of the orientational disorder in the solid makes the LDS stable up to higher temperatures. However, it is important to stress that the appearance of the LDS in the phase diagram is not due to the orientational disorder contribution. Since this contribution is also present in the HDS and takes the same value, it does not alter the relative stabilities of the LDS and the HDS. Nevertheless, the stability of both phases with respect to the fluid does depend on this contribution and this affects the location of the fluid–LDS–HDS triple point temperature.

Finally, we present results obtained from the cell theory for the PMW model with  $\lambda^* = 0.15$ . In Table III the free energies obtained from the free energy calculations of this work are compared with the free energies obtained from the cell theory. The agreement is reasonably good. In Fig. 11 the EOS for the solid phases as obtained from MC simulation is compared with the EOS as obtained from the cell theory. The agreement between theory and simulation is reasonably good given the simplicity of the cell theory. The cell theory seems to work better for the high-density solid than for the LDS. The way in which the zero pressure is achieved by the cell theory deserves some comment. In fact according to Eq. (23) the free energy is given by the lattice energy and the free volume (i.e.,  $q_1$ ). Since the lattice energy does not depend on density for densities higher than those given by Eq. (2) then

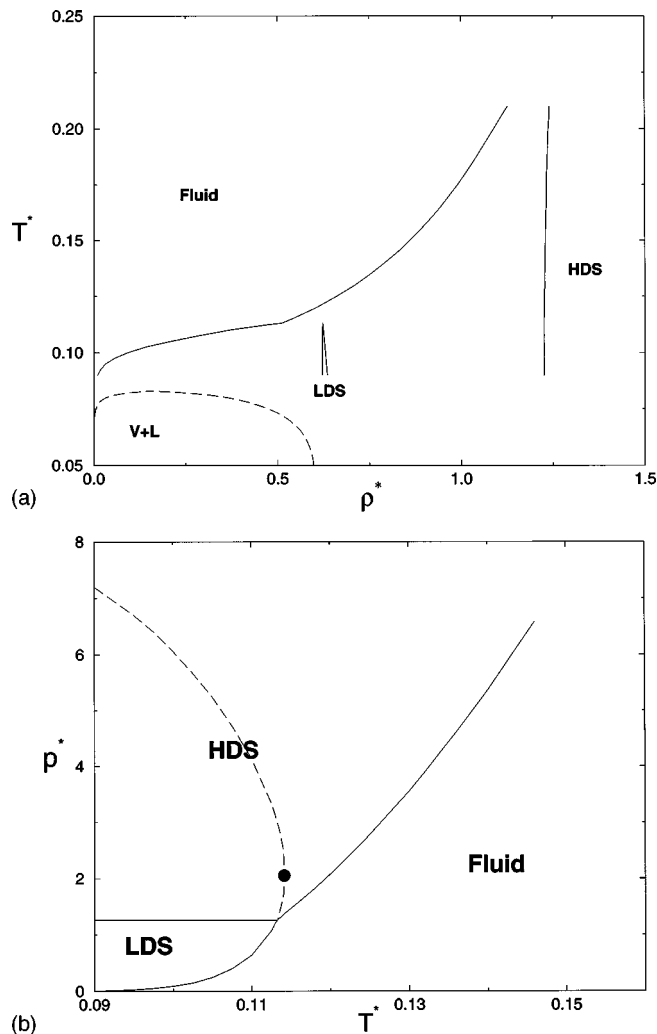


FIG. 9. Phase diagram for the PMW model with  $\lambda^* = 0.10$ . (a)  $T^* - \rho^*$  diagram. The vapor–liquid equilibrium predicted by the Wertheim theory is represented by the dashed line. The densities of the LDS in the LDS–HDS solid transition have been slightly incremented with respect to the actual values for visual clarity. (b)  $\rho^* - T^*$  diagram showing the region of stability of each phase. The triple point where the three solid lines meet correspond to  $T^* = 0.1125$  and  $\rho^* = 1.20$ . The dashed line indicates a phase transition between the metastable fluid and the metastable LDS. The filled circle indicates the state where the transition between the metastable phases occurs without density change.

the only density dependence of the free energy is given by the free volume. The existence of the solid at zero pressure requires according to the cell theory the existence of a minimum in the free volume. This is indeed the case. For the PMW the free volume is essentially the volume for bonding of a central molecule with four of its neighbors. At high densities the decrease of the density provokes an increase in the free volume. This is so because the region for bonding around each bonding site (an imaginary sphere of radius  $\lambda^*/2$ ) lies partially within the neighbor hard sphere cores. Decreasing the density takes part of this region out of the neighbor hard sphere cores. Therefore, the free volume increases as the density decreases. At low densities, the region for bonding around each bonding site does not penetrate any of the nearest neighbors hard spheres in the perfect lattice. Decreasing the density in this case, decreases the free vol-

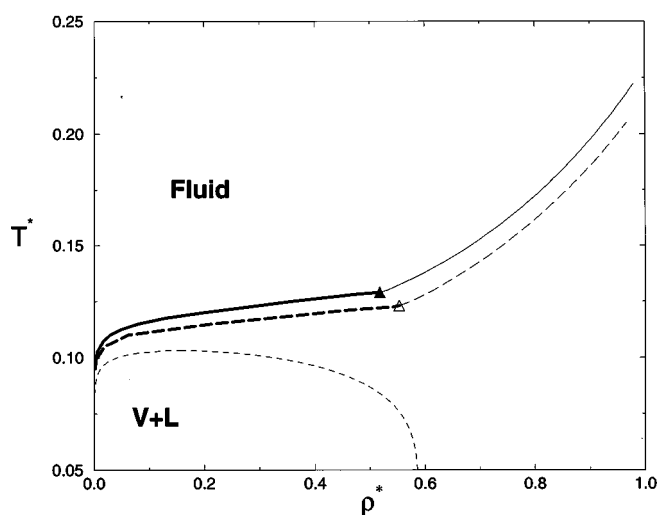


FIG. 10. Fluid densities at freezing for the PMW model with  $\lambda^*=0.15$  when the orientational disorder contribution [Eq. (11)] of the solid is included (solid lines) or when it is not included (dashed lines). Thick lines fluid-LDS transition. Thin lines fluid-HDS transition. The triangle represents the temperature of the triple point when the orientational disorder contribution is included (filled triangle) or when it is not included (open triangle). The vapor-liquid coexistence curve (small dash line) obtained from the Wertheim theory is also shown.

ume, since the central molecule has less volume for bonding simultaneously to four of the neighbors. Not surprisingly the density at zero pressure for all the models and solid structures, corresponds approximately to the arithmetic average of the close packed density and the nonbonding density [as given by Eq. (2)]. For instance for the HDS solid of the model with  $\lambda^*=0.15$  the density at zero pressure from MC simulations is of about 1.16. The average of the close-packed density and the nonbonding density [see Eq. (2)] yields 1.14 in reasonable agreement.

It is worthwhile to make a few additional comments about the low-temperature fluid behavior in this model. As mentioned earlier Wertheim's theory predicts a vapor-liquid coexistence region for the model at states where such behavior is preempted by the solid-fluid transitions. Figures 12 and 13 show the EOS obtained from the Wertheim theory compared with Monte Carlo simulations at  $T^*=0.12$  and  $T^*=0.10$ . We see that the agreement between theory and simulation is good at low densities to moderate densities and, in particular, for the states where our phase equilibrium calculations show the fluid to be stable with respect to solid phases. On the other hand, the agreement deteriorates at high densities. Unlike the case at higher temperatures discussed earlier these low-temperature simulation results exhibit hysteresis between isotherms generated by expansion and those

TABLE III. Free energy as determined from the Monte Carlo simulations and from cell theory.

Solid	$\lambda^*$	$T^*$	$\rho^*$	$A_{\text{ref}}/(NkT)$	$A_{\text{cell}}/(NkT)$
LDS	0.15	0.12	0.60	-2.4636	-2.1133
HDS	0.15	0.12	1.171	-1.7177	-2.0104
HDS	0.15	0.12	1.240	-0.6021	-0.2780

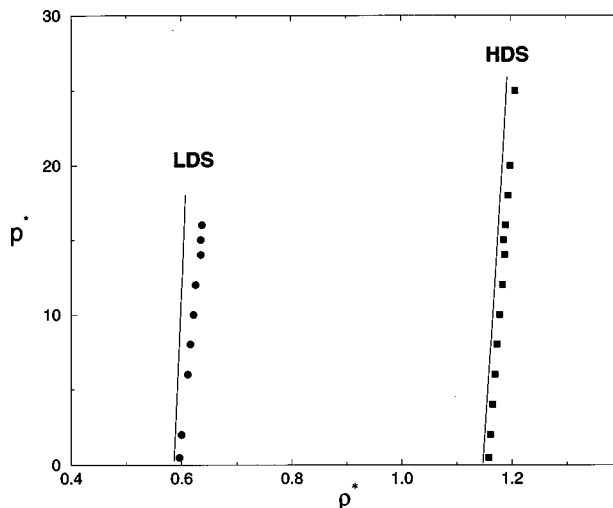


FIG. 11. Pressure vs density for the PMW with  $\lambda^*=0.15$  and  $T^*=0.12$  as obtained from simulation (symbols) and from the cell theory (lines). Results for the LDS (filled circles and solid line on the left) and for the HDS (filled squares and solid line in the right).

generated by compression, especially at the lower temperature. This hysteresis is caused by the strong square well bond network formed at high density. Once a network is established, fluctuations in the connectivity are rare events. Notice that at the lower temperature expansion from the dense fluid state leads to states of large negative pressure. In this respect the system seems to be exhibiting the elasticity effects seen in polymer networks.<sup>41</sup> Negative pressures are only seen in the Wertheim theory at significantly lower temperature (results for  $T^*=0.06$  are also shown in Fig. 13) as part of the van der Waals loops which accompany analytical expressions for the free energy of a fluid with attractive forces. Attempts to simulate vapor-liquid equilibrium by using the

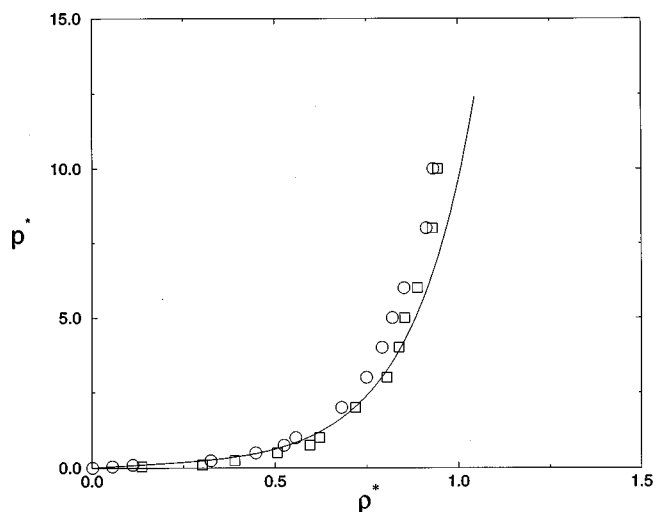


FIG. 12. Pressure vs density for the PMW model with  $\lambda^*=0.15$  at  $T^*=0.12$ . Open circles: MC results obtained by compressing a low-density state. Open squares: MC results obtained by expansion. Solid line: Results from Wertheim EOS. The simulations were performed with 128 molecules, and run over 25.6 million configurations with half of these used for equilibration. The high-density fluid obtained from compression was the initial state for the expansion.

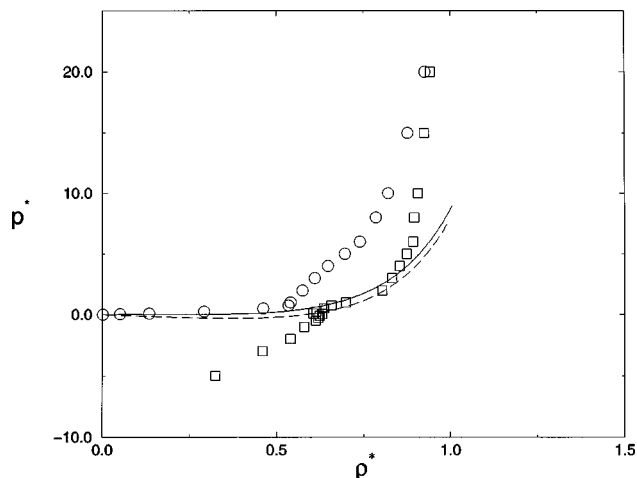


FIG. 13. Pressure vs density for the PMW model with  $\lambda^*=0.15$  at  $T^*=0.10$ . Open circles: MC results obtained by compressing a low-density state. Open squares: MC results obtained by expansion. Solid line: Results from Wertheim EOS for  $T^*=0.10$ . Dashed line: Results from Wertheim EOS for  $T^*=0.06$ . The simulations were performed with 64 molecules, and run over 7.68 million configurations with half of these used for equilibration. The high-density fluid obtained from compression was the initial state for the expansion.

Gibbs ensemble<sup>42</sup> were unsuccessful. We are led to the conclusion that these low-temperature metastable fluid states are vitreous in character and that vapor–liquid coexistence may not be observable even as a metastable equilibrium.

## V. CONCLUSIONS

We have presented a study of the solid–fluid equilibrium in the PMW using Monte Carlo simulation and theory. Several conclusions can be drawn from our results:

- (1) The short-range directional forces in this model introduce a LDS phase (similar to ice Ic) into the phase diagram.
- (2) When considering only the fluid and the LDS phases we found re-entrant behavior. Melting from the LDS to a higher density fluid occurs. We believe that this behavior is similar to that of low coordination solid phases such as those of water.
- (3) When the HDS is considered then it is observed that the LDS to high-density fluid transition is preempted by a transition to the HDS. Tetrahedral short-range coordination is sufficient to stabilize a low-density solid, but this is not enough to lead to melting from this solid to a higher density liquid. This suggests that the traditional view of the “anomalous” melting of ice to a high-density fluid as being due to the “open structure” of ice should be revised.
- (4) From the present study it appears that in order for re-entrant melting to occur, solid phases with high density and tetrahedral coordination (e.g., our HDS phase) must be made less stable. It seems likely that introducing a nonspherical core or introducing saturation within the model (with strong repulsion with nonbonded nearest neighbors) as has been done by Speedy<sup>17</sup> will act to destabilize the HDS phase.

- (5) The existence of orientational disorder in the solid is not needed for the presence of the LDS in the phase diagram. Neither is it a determining factor for the existence of melting to a high-density fluid. However, the orientational disorder increases the temperature range where the solid phases are stable with respect to the fluid.
- (6) The PMW does not exhibit a true vapor–liquid equilibrium. The condensation of the low-density fluid (vapor) to a high-density fluid (liquid) is preempted by solidification. This is similar to what has been found for systems with spherically symmetric short range interactions.<sup>39</sup>
- (7) Wertheim’s thermodynamic perturbation theory is quite successful in describing the fluid phase of the PMW under the conditions where it is stable with respect to solidification. For the solid phase the cell theory gives a fair description of the equation of state and free energies.

## ACKNOWLEDGMENTS

This work was supported by the U.S. Department of Energy, Office of Basic Energy Sciences (DE-FG02-90ER14150) to P.A.M., by project PB97-0329 of the DGICYT of Spain to C.V. and by a cooperative research grant from NATO (CRG. 970275).

- <sup>1</sup>W. G. Hoover and F. Ree, *J. Chem. Phys.* **49**, 3609 (1968).
- <sup>2</sup>J. P. Hansen and L. Verlet, *Phys. Rev.* **184**, 151 (1969).
- <sup>3</sup>B. Mulder and D. Frenkel, *Mol. Phys.* **55**, 1171 (1985).
- <sup>4</sup>S. C. McGrother, D. C. Williamson, and G. Jackson, *J. Chem. Phys.* **104**, 6755 (1996).
- <sup>5</sup>P. Bolhuis and D. Frenkel, *J. Chem. Phys.* **106**, 666 (1997).
- <sup>6</sup>S. J. Singer and R. Mumaugh, *J. Chem. Phys.* **93**, 1278 (1990).
- <sup>7</sup>C. Vega, E. P. A. Paras, and P. A. Monson, *J. Chem. Phys.* **96**, 9060 (1992).
- <sup>8</sup>C. Vega, E. P. A. Paras, and P. A. Monson, *J. Chem. Phys.* **97**, 8543 (1992).
- <sup>9</sup>C. Vega and P. A. Monson, *J. Chem. Phys.* **107**, 2696 (1997).
- <sup>10</sup>C. Vega and P. A. Monson, *J. Chem. Phys.* **102**, 1361 (1995).
- <sup>11</sup>W. N. Shen and P. A. Monson, *J. Chem. Phys.* **103**, 9756 (1995).
- <sup>12</sup>C. Vega, F. Bresme, and J. L. F. Abascal, *Phys. Rev. E* **54**, 2746 (1996).
- <sup>13</sup>A. Malanoski and P. A. Monson, *J. Chem. Phys.* **107**, 6899 (1997).
- <sup>14</sup>I. M. Svishchev and P. G. Kusalik, *Phys. Rev. Lett.* **73**, 975 (1994).
- <sup>15</sup>L. A. Baez and P. Clancy, *J. Chem. Phys.* **103**, 9744 (1995).
- <sup>16</sup>L. A. Baez and P. Clancy, *Mol. Phys.* **86**, 385 (1995).
- <sup>17</sup>R. J. Speedy, *J. Chem. Phys.* **107**, 3222 (1997).
- <sup>18</sup>J. Kolafa and I. Nezbeda, *Mol. Phys.* **61**, 161 (1987).
- <sup>19</sup>I. Nezbeda, J. Kolafa, and Y. V. Kalyuzhnyi, *Mol. Phys.* **68**, 143 (1989).
- <sup>20</sup>I. Nezbeda and G. A. Iglesias-Silva, *Mol. Phys.* **69**, 767 (1990).
- <sup>21</sup>J. Kolafa and I. Nezbeda, *Mol. Phys.* **72**, 777 (1991).
- <sup>22</sup>I. Nezbeda, J. Kolafa, J. Pavlicek, and W. R. Smith, *J. Chem. Phys.* **102**, 9638 (1995).
- <sup>23</sup>M. S. Wertheim, *J. Stat. Phys.* **35**, 19 (1984).
- <sup>24</sup>M. S. Wertheim, *J. Stat. Phys.* **35**, 35 (1984).
- <sup>25</sup>D. Ghonasgi and W. G. Chapman, *Mol. Phys.* **79**, 291 (1993).
- <sup>26</sup>J. A. Barker, *Lattice Theories of the Liquid State* (Pergamon, New York, 1963).
- <sup>27</sup>X. Cottin and P. A. Monson, *J. Chem. Phys.* **99**, 8914 (1993).
- <sup>28</sup>X. Cottin and P. A. Monson, *J. Chem. Phys.* **102**, 3354 (1995).
- <sup>29</sup>E. P. A. Paras, C. Vega, and P. A. Monson, *Mol. Phys.* **77**, 803 (1992).
- <sup>30</sup>C. Vega and P. A. Monson, *Mol. Phys.* **85**, 413 (1995).
- <sup>31</sup>D. Eisenberg and W. Kauzmann, *The Structure and Properties of Water* (Oxford University Press, New York, 1969).

- <sup>32</sup>Edited by R. A. Horne, *Water and Aqueous Solutions* (Wiley, New York, 1972).
- <sup>33</sup>H. Tanaka, J. Chem. Phys. **108**, 4887 (1998).
- <sup>34</sup>D. Frenkel and J. A. C. Ladd, J. Chem. Phys. **81**, 3188 (1984).
- <sup>35</sup>B. Kamb, J. Chem. Phys. **43**, 3917 (1965).
- <sup>36</sup>C. G. Gray and K. E. Gubbins, *Theory of Molecular Fluids* (Clarendon, Oxford 1984).
- <sup>37</sup>L. Pauling, J. Am. Chem. Soc. **57**, 2680 (1935).
- <sup>38</sup>J. F. Nagle, J. Math. Phys. **7**, 1484 (1966).
- <sup>39</sup>M. H. J. Hagen and D. Frenkel, J. Chem. Phys. **101**, 4093 (1994); P. Bolhuis and D. Frenkel, Phys. Rev. Lett. **101**, 9869 (1994); P. Bolhuis, M. Hagen, and D. Frenkel, Phys. Rev. E. **50**, 4880 (1994).
- <sup>40</sup>Using the Gibbs–Helmholtz equation we can show that if the configurational energy is a constant then  $(\partial(A^c/T)/\partial(1/T))_{V,N}$  is independent of density. It follows that  $p/T = -(\partial(A^c/T)/\partial V)_{T,N}$  is independent of temperature.
- <sup>41</sup>F. A. Escobedo and J. J. de Pablo, J. Chem. Phys. **106**, 793 (1997); Mol. Phys. **90**, 437 (1997).
- <sup>42</sup>A. Z. Panagiotopoulos, Mol. Phys. **61**, 813 (1987).